

TESTING COMPTONIZATION MODELS USING BEPPoSAX OBSERVATIONS OF SEYFERT 1 GALAXIES

P.O. PETRUCCI^{1,2}, F. HAARDT², L. MARASCHI¹, P. GRANDI³, J. MALZAC¹, G. MATT⁶, F.
NICASTRO^{3,4,5}, L. PIRO³, G.C. PEROLA⁶, A. DE ROSA³.

Draft version October 26, 2018

ABSTRACT

We have used realistic Comptonization models to fit high quality BeppoSAX data of 6 Seyfert galaxies. Our main effort was to adopt a Comptonization model taking into account the anisotropy of the soft photon field. The most important consequence is a reduction of the first scattering order, which produces a break (the so-called anisotropy break) in the outgoing spectra. Thus anisotropic Comptonization models yield spectra with convex curvature. The physical parameters of the hot corona (i.e. the temperature and optical depth) obtained fitting this class of models to broad band X-ray spectra are substantially different from those derived fitting the same data with the power law + cut-off model commonly used in the literature. In particular, our best fits with Comptonization models in slab geometry give a temperature generally much larger and an optical depth much smaller than derived from the power law + cut-off fits, using standard Comptonization formulae. The estimate of the reflection normalization is also larger with the slab corona model. For most objects of our sample, both models give Compton parameter values larger than expected in a slab corona geometry, suggesting a more “photon starved” X-ray source configuration. Finally, the two models provide different trends and correlation between the physical parameters: for instance, with the power law + cut-off fits, we obtain a correlation between the reflection normalization and the corona temperature whereas we find an anti-correlation between these parameters with the slab geometry. These differences have major consequences for the physical interpretation of the data. In the framework of reprocessing models, the cut-off power law best fit results suggest the thermal corona to be dominated by electron-positron pairs. On the contrary, the slab corona model is in better agreement with a low pair density solution.

Subject headings: galaxies: active; galaxies: Seyfert; X-rays: galaxies

1. INTRODUCTION

The broad band X-ray spectra (2-300 keV) of Seyfert 1 galaxies are generally well fitted by a cut-off power law continuum with superimposed secondary components like a neutral iron line and a reflection hump. The latter components have been detected in the end of the eighties with GINGA (Piro et al. 1990; Matsuoka et al. 1990; Pounds et al. 1990) and are considered as signatures of reprocessing of the primary X-ray emission in surrounding cold matter. A high energy cut-off in the X-ray/ γ -ray part of the spectrum was first unambiguously detected by SIGMA and OSSE in NGC 4151 (Jourdain et al., 1992; Maisack et al. 1993). A high energy cut-off was also requested to fit the average X-ray/ γ -ray spectra (obtained from data of different satellites) of a sample of Seyfert (Zdziarski et al. 1995; Gondek et al. 1996). The broad band capabilities of the Italian-Dutch satellite BeppoSAX allowed to detect high energy cut-offs in other Seyfert 1 galaxies, about half of the fifteen observed with this satellite. Values of the high energy cut-offs range from 70 keV to ~ 300 keV (Matt 2000, hereafter M00).

A cut-off power law plus reflection model (the so-called

PEXRAV model in XSPEC, Magdziarz & Zdziarski 1995) depends on three parameters: the spectral index Γ , the high energy cut-off E_c and the reflection normalization R , the formers characterizing the shape of the primary continuum. The physical interpretation of these parameters is generally done in the framework of thermal Comptonization mechanism, which is commonly believed to be the origin of the X-ray emission of Seyfert galaxies. Using approximate relations (cf. section 4), it is then possible to derive, from values of Γ and E_c , values of the temperature kT_e and optical depth τ of the “comptonizing” hot plasma (the so-called corona).

If such approximations are sufficient in isotropic geometries (e.g. a central soft photon source surrounded by a spherical hot cloud), where Comptonization process produces roughly power law spectra with a high energy cut-off, strong discrepancies may appear in anisotropic ones, especially for small optical depth and large temperature. Indeed, the (possible) anisotropy of the source of seed photons (as seen by the corona), may introduce anisotropies and modifications of the outgoing spectrum. The largest effect occurs when soft photons are emitted

¹Osservatorio Astronomico di Brera, Milano, Italy

²Università dell’Insubria, Como, Italy

³IAS/CNR, Roma, Italy

⁴CfA, Cambridge Ma., USA

⁵Osservatorio Astronomico di Roma, Roma, Italy

⁶Università degli Studi “Roma 3”, Roma, Italy

by a plane (disk) below the corona. In this case, photons backscattered towards the disk in the first scattering are necessarily produced in "head-on collisions" and therefore have an energy gain larger than average, while photons scattered towards the corona (i.e. in the forward direction) have an energy gain smaller than average. As a consequence, the contribution of the first scattering order to the outgoing flux is significantly reduced producing a spectral break (the so-called anisotropy break) in the spectrum. Below the high energy cut-off the spectra is then better described by broken power laws than by a simple power law contrary to what is generally believed (Petrucchi et al., 2000, hereafter P00). These anisotropic effects become however less important for larger optical depth (i.e. $\tau > 1$) since they are "smoothed" by the larger number of Compton scatterings suffered by the soft photons.

It is also worth noting that the energy of the anisotropy break which is, in practice, close to the peak energy of the third scattering order (Haardt 1993), depends on kT_e but also on the temperature of the seed soft photon plasma kT_{bb} . Consequently, if in the case of isotropic geometry the spectral shape is relatively independent on kT_{bb} , which fixes only the low energy boundary of the emitted spectrum, in anisotropic geometry the shape of the Comptonization spectra depends on it.

In a recent paper (P00), we have applied accurate Comptonization models to fit high quality data of the *BeppoSAX* long look at NGC 5548. We have underlined the importance of the anisotropic effects and, in particular, we have shown that due to the presence of the anisotropy break, above which the intrinsic continuum is steeper, the temperature of the hot electrons estimated from Comptonization models in anisotropic geometry can be much larger than the one derived fitting the data with a power-law + cut off model.

Besides, we have shown that these different models may provide different (and even opposite) relationships between physical parameters. For instance, still in the case of NGC 5548, the spectral softening of the spectrum, observed during a small flare in the central part of the observation, goes with an increase of the high energy cut-off (i.e. of the corona temperature), in the case of PEXRAV, but with a decrease of the corona temperature when using an anisotropic Comptonization model.

In the same spirit of P00, we extend our application of accurate Comptonization models to a larger sample of objects. We report in this paper the results of this study. The paper is organized as follows. In section 2 we briefly present the main results of the *BeppoSAX* observations of Seyfert galaxies. We also present the sample of objects we use for the purpose of this paper. We describe the models we used and the fitting procedure in section 3. We also detail in this section the fit of the soft excess/warm absorber (hereafter WA) features observed in each object. We present the results of the fits in section 4 and discuss their physical interpretations in section 5. We then conclude in the last section.

2. THE DATA

2.1. Overview of the *BeppoSAX* observations of Seyfert 1 galaxies

Two major *BeppoSAX* Core programs were devoted to classical Seyfert 1 galaxies aiming to study the broad band spectra (PI: G.C. Perola) and spectral variability (PI: L. Piro). Thirteen sources have been observed on aggregate so far, since the launch of the satellite in 1996.

Reviews summarizing the main results on these sources have been presented by Piro et al., (1999) and M00. For all objects, the spectral models used by the authors included a power law with exponential cut-off (i.e. $f_E \propto E^{1-\Gamma} e^{-E/E_c}$) characterized by a photon index Γ and a e-folding energy E_c , a gaussian to fit the neutral Iron line near 6.4 keV and a Compton reflection continuum characterized by a reflection normalization R . Soft excess and/or WA features were added if required by the data.

The major findings are the followings:

- A high energy cut-off is generally observed, with an e-folding energy typically in the range 70–300 keV.
- All sources show the presence of a reflection component, so confirming the GINGA and ASCA results (Nandra & Pounds, 1994).
- Only two objects (Mkn 509 and Mkn 841) show the presence of a soft excess. This sharply contrasts with the results obtained with EXOSAT (Turner & Pounds 1989) or ROSAT (Walter & Fink, 1993) where most of the Seyfert 1 observed seemed to show such excess (for a discussion of this point see Piro et al., 1997). On the other hand, WA features (mostly the O VII and O VIII edges) are generally observed in the LECS range.
- A correlation between the power law index Γ and the amount of reflection component R is indicated, in the same sense as found by Zdziarski et al. (1999, hereafter Z99). However, the issue of the reality of this correlation is still open since it may be due to the fact that the two parameters are strongly related in the fitting procedure (see for example Vaughan & Edelson 2000).

2.2. Our sample

From the sample of Seyfert 1 galaxies observed by *BeppoSAX*, we have selected observations with good signal-to-noise ratios at high energies as measured with the PDS instrument. We therefore favored objects with hard X-ray spectra. Such observations are best suited for an analysis of the high energy spectra.

The subsample of objects studied in this paper is reported in Table 1, with the name of the different objects, the date of the *BeppoSAX* observations (some of these objects have been observed several times), the exposure time and the statistical significance in the PDS instrument. We also present results from the observation of ESO 141-G55, even if its detection in the PDS instrument is relatively weak, since this source was recently observed for the first time by *BeppoSAX*.

NGC 4151 was observed three times by *BeppoSAX*, two times in 1996 during the SV-phase (in July and in December), and the last one in January 1999 during A02. However during the observation of July 96, the source experienced a strong increase of the 2-10 keV flux by a factor two on time scales of one day, with significant spectral variability as shown by Piro et al. (2000a). According to these authors, we choose to study separately the low and high state occurring during this period (and indicated as 96L and 96H in the following). Unfortunately, during the high state, the LECS was off. Only the MECS and PDS data are therefore available for this state. We have not used, in this paper, the observation of December 96 since it does not differ substantially from the low state of July 96.

Concerning Mkn 509, its observation has been split in two parts during the AO2. Since no significant spectral variability was observed between the two data sets (Perola et al. 2000), we will only refer here to the combined spectrum.

In this paper, we will be concerned with data from three of the four instruments on board *BeppoSAX*: the Low Energy Concentrator Spectrometer, LECS (Parmar et al. 1997) covering the 0.15–10 keV range, the Medium Energy Concentrator Spectrometer, MECS (Boella et al. 1997) covering the 2–10 keV range and the Phoswich detector system, PDS (Frontera et al. 1997) covering the range 13 – 200 keV. Due to some problems that remain in the spectral analysis of LECS data above 4 keV, we shall use only data in the range 0.1–4 keV.

LECS and MECS event files and PDS pha files were downloaded from the *BeppoSAX* SDC archives. The spectral counts were extracted from a circular region of 4' and 8' radius around the source centroid in the MECS and LECS images respectively. We used the data of the three (or two, for observations done after May 1997) MECS units merged together to increase the signal-to-noise ratio. In XSPEC (Arnaud 1996), we use the last updated responses (Sep. 1997) and background matrices of each instrument.

3. MODEL FITTING

3.1. The primary continuum

We fit the data using two different models for the primary continuum: 1) an exponentially cut-off power law plus a reflection component from neutral material (PEXRAV model of XSPEC, Magdziarz & Zdziarski 1995) and 2) a thermal Comptonization spectrum from a disk+corona configuration in slab geometry. The latter was obtained using the code of Haardt (1994, hereafter we will refer to this Anisotropic Comptonization Code as AC2). This code derived the angle-dependent spectra of the disk-corona system using an iterative scattering method, where the scattering anisotropy was taken into account only in the first scattering order. It includes also a reflection component described following White, Lightman & Zdziarski (1988) and Lightman & White (1988) and assuming neutral matter. The spectral shape of the

reflected photons is averaged over angles. It is multiplied by a first normalization factor which depends on the inclination angle (see Ghisellini, Haardt & Matt 1994 for details). In addition, the usual R normalization is left free to vary in the fit procedure, so that, for the given inclination angle, $R = 1$ corresponds to a solid angle, subtended by the reflector, of 2π . We do not apply Comptonization models for other geometries (e.g. hemisphere) since, as shown for NGC 5548 (P00), the results follow closely those obtained with the slab geometry.

The fit parameters of AC2 are the temperature of the corona kT_e , its optical depth τ , the temperature of the disk kT_{bb} (assuming a black body soft emission) and the reflection normalization R . On the other hand, the PEXRAV continuum depends only on 3 parameters: the e-folding energy of the cut-off power law E_c , the photon index Γ and the reflection normalization R .

3.2. Soft X-ray excess and Warm Absorber

Most of the objects present WA features and/or a Soft excess in the low part (i.e. in the LECS energy band) of their spectra. Good and realistic fits require to take these features into account. Detailed analyses of these different components are however beyond the scope of this paper, which is instead focused on the high energy continuum of the sources. Then, as a first approximation, we have added simple components (edges, gaussian, blackbody...) to the primary continuum to reproduce the main features present in the soft part of the spectra. We discuss briefly the case of each source in the following.

3.2.1. NGC 4151

The *BeppoSAX* data of this galaxy have already been analyzed by Piro et al. (2000a, 2000b), assuming a simple cut-off power law for the primary underlying continuum. A prominent soft excess, known to exist in this object (Holt et al. 1980) below the ~ 2 keV cutoff due to a high absorbing column, is clearly detected in the observations of 1996 (low state) and 1999. It is generally modeled by allowing some fraction of the central source to be completely uncovered or viewed through a lower column (the so-called “leaky absorber”). In addition, there is evidence of a possibly separate soft excess component that does not vary with the 2–10 keV continuum (Pounds et al., 1986; Perola et al., 1986). Part of this emission comes from an extended X-ray region known to exist in this object (Elvis et al. 1983; Morse et al. 1995). Recent Chandra observations with the High Energy Transmission Grating Spectrometer have revealed detail spectra of this source (Ogle et al., 2000) and allow for the first time precise measurements of the ionization, temperature and kinetics of the extended soft X-ray emission region.

For the scope of the present paper, we model the complex soft X-ray emission in a (relatively) simpler manner. According to Piro et al. (2000a 2000b), we have used a dual absorber that is the source is covered completely by a medium with a column density N_{H1} and with a covering fraction f_{cov} by a second medium with a column density N_{Hcov} . On the other hand, the soft excess below 2 keV

was modeled by a scattering component plus an ultrasoft component described by a thermal bremsstrahlung, both absorbed by the galactic column density.

Due to the lack of LECS data for the high state of 1996, we cannot constrain the different components of the soft X-ray range. We thus analyze the data only above 3.5 keV adding a simple photo-electric absorption characterized by a column density N_{H1} .

We have reported for the three observations our best fit parameters N_{H1} , N_{Hcov} and f_{cov} , obtained with PEXRAV to model the continuum, in Table 3. We note a significant increase of N_{H1} between 96L and 99. As already noted by Piro et al (2000a, 2000b), such variations suggest that the structure of the dual absorber has slightly changed between the two observations.

3.2.2. NGC 3783

Evidences for deep absorption features in the 0.1-1.5 keV band of NGC 3783 have already been detected in ROSAT (Turner et al. 1993) and ASCA observations (George et al. 1995), the main ones being the O VII and O VIII edges at 0.74 and 0.87 keV respectively. More recently, in January 2000, NGC 3783 was observed using the High Energy Transmission Grating Spectrometer on the Chandra X-ray observatory (Kaspi et al., 2000). These authors detected a large number of emission and absorption lines, strongly confirming the presence of warm absorbing/emitting media embedding the central X-ray source.

An emission feature near 0.5 keV has also been claimed in ASCA spectra of this source (George et al. 1998) and has been interpreted as an O VII emission line (expected at 568 eV). Kaspi et al. (2000) clearly see this emission feature in the Chandra spectra, confirming for the first time the detection of this component.

According to these results, we have included in our models two absorption edges, near 0.74 and 0.87 keV, and a gaussian peaking near 0.5 keV to fit the O VII line. The best fit results are reported in Table 2. As suggested by the recent observation of Chandra, the edge near 1.3-1.4 likely corresponds to contributions by Fe L and Ne K edges whereas the second one, centered near 0.8-0.9 keV, may be due to the O VIII edge.

Concerning the line, we have checked that its addition significantly improves the fit with $\Delta\chi^2=16$ (according to the F-test, this difference implies a probability less than 0.01 that the line is due to random fluctuations in the counts). This feature is thus detected by *BeppoSAX* with a high confidence level. The corresponding best fit central energy of the line was $E_{line} \simeq 0.55$ keV with an EW of ~ 100 eV. Such EW is large, and it is unlikely that this emission features was only produced by O VII emission lines. In fact, in the more extreme case where we see the blends of the three O VII lines, we expect an EW of only 30 eV (De Rosa, private communication). The large EW and small energy of the line we obtained can be due in part to a bad modeling of the continuum near this component.

3.2.3. Mkn 509

Mkn 509 was observed by *BeppoSAX* in 1998. The observation was split in two parts during the AO2, the first one being done in May 1998 and the second one in October 1998. As already said, a hardness ratio analysis of the counts shows marginal evidence of spectral variations between the two observations. They have thus been combined and we applied the spectral analysis to the integrated counts.

These data have already been studied in detail by Perola et al. (2000, hereafter PER00). Assuming a cut-off power law model for the intrinsic continuum of this source, the data show at low energy the presence of additional, superimposed features due to O VII and/or O VIII edges as well as a strong soft excess. PER00 described the latter by a “soft” power law component ($A_s E^{-\Gamma_s}$). They then obtained a significant improvement of the goodness of the fit ($\Delta\chi^2=20$), the best fit values for A_s and Γ_s being $1.11 \times 10^{-2} \text{ cm}^{-2} \text{ sec}^{-1} \text{ keV}^{-1}$ and 2.5 respectively.

PER00 underlined the fact that the addition of this “soft” component had also the interesting effect of providing a more astrophysically sound global solution, with a reflection normalization $R \sim 0.6$ and Iron line width $\sigma_{Fe} \sim 0.4$ keV (compared to $R \simeq 2$ and $\sigma_{Fe} \sim 3$ keV without this soft component), giving some confidence on the correctness of the model.

Following these authors, we have added this “soft” power law to our fit, fixing A_s and Γ_s to the best fit values given above. We also add an edge with the best fit energy and optical depth found by PER00, i.e. $E_{edge} = 0.74$ keV, $\tau_{edge} = 0.06$.

3.2.4. ESO 141-G55

The presence of a soft excess was already suggested for this source from ROSAT observations (Turner et al 1993). However the *BeppoSAX* data do not show any evidence of such component nor WA features. It could be partly due to the low S/N of this observation. Consequently, our fits were done without any additional components in the soft band other than the absorption by the galactic column density (cf. Tables 3 and 4).

3.2.5. NGC 5548

The WA observed in this source was already discussed in P00 and Nicastro et al. (2000) and the reader can refer to these papers for more details. For the purpose of this work, we adopt the results of P00 who have added two edges, at $E_1 = 0.74$ keV and $E_2 = 0.87$ keV, to fit the Oxygen absorption features observed in the LECS band. The corresponding optical depths were fixed to the best fit values obtained with PEXRAV, i.e. $\tau_1 = 0.51$ and $\tau_2 = 0.12$ respectively.

3.2.6. IC 4329A

The X-ray spectrum of IC 4329A is known to display strong neutral absorption, below 3 keV, due to a gas column about ten times greater than the galactic value $N_{gal} = 4.5 \times 10^{20} \text{ cm}^{-2}$ (Elvis et al. 1989). This gas is

supposed to be associated with the disk of the host galaxy, which is oriented nearly edge-on (Petre et al. 1984).

At low energies (below 1-2 keV), ROSAT and ASCA observations have also shown evidence of two rather strong edges, one consistent with O VII, the other with O VIII (Madejski et al. 1995; Cappi et al., 1996; Reynold 1997; George et al. 1998).

The *BeppoSAX* observation of IC 4329A has been already analyzed by Perola et al. (1999) using PEXRAV as primary continuum. To model the soft range of the spectrum, they added a neutral column of gas in addition to the galactic one and included two absorption edges. This model gives a good fit to the data and we adopt the same description in our fits. We fix the energy and optical depth of the two edges and the neutral column density to the best fit values obtained by Perola et al. (1999), i.e. $E_1 = 0.73$ keV, $\tau_1 = 0.52$, $E_2 = 1.03$ keV, $\tau_2 = 0.19$ and $N_h = 0.38 \times 10^{22} \text{ cm}^{-2}$.

3.3. Fitting procedure

Since the sample is only composed of Seyfert 1 galaxies, we expect, in the unification model framework, relatively small inclination angles. In the case of NGC 4151, there are claims of a large inclination angle ($\sim 60^\circ$, Evans et al. 1993). However this value is rather uncertain. To reduce the length of the fitting procedure, we thus decided to fix, for all the objects of our sample, the inclination to 30° (Nandra et al. 1997).

The geometrical normalization of the reflection component R was let free to vary. We recall that a value $R = 1$ corresponds to a covering factor of the cold matter to the X-ray source of $\Omega = 2\pi$ whatever the degree of anisotropy of the X-ray emission.

We added a gaussian to reproduce the iron line complex near 6.4 keV. The central energy and width of the gaussian were let free to vary. An Iron edge in the range 7–9 keV was also added if required by the data, that is for NGC 4151, NGC 3783.

We allowed the relative MECS to PDS normalization to vary by 5% around the value of 0.86 to account for the estimated systematic uncertainty (Fiore et al. 1999). Analogously, we let the LECS to MECS normalization free to vary over the range of acceptable values 0.7–1 (Fiore et al. 1999).

Finally, in the case of PEXRAV, we fixed the parameters of the soft excess and/or WA components (i.e. edges, line, soft power law) to the values presented in section 3.2. For fits with AC2, we also fixed, in a first step, the column density to the best fit values obtained with PEXRAV. A second series of fits were obtained with a column density free to vary. We checked that there were no significant differences between the two sets of results (we generally obtain slightly larger column densities and changes of the soft temperature kT_{bb} when N_h is let free to vary). We will thus only consider the best fit results with free column density in the following.

For computing errors on the parameters of the primary

continuum (that is kT_e , τ , kT_{bb} and R for AC2, and E_c , Γ and R for PEXRAV), we let the column density free to vary but we fixed the LECS/MECS and MECS/PDS normalization, and the Iron line and/or edges to their best fit values. Throughout the paper, errors on single parameter are quoted at a confidence level of 90 % (i.e. $\Delta\chi^2=2.7$) unless otherwise specified.

4. RESULTS

4.1. The PEXRAV model

The best fit parameter values obtained with the fitting procedure described above using the PEXRAV model are reported in Table 3. We checked, as far as possible, our PEXRAV results with those already published on these data. For IC 4329A, Mkn 509, NGC 4151, NGC 3783 and NGC 5548 our PEXRAV fits are in good agreement with those obtained by Perola et al. (1999), Perola et al. (2000), Piro et al. (2000a, 2000b), De Rosa et al. (2000) and Nicastro et al. (2000) respectively. In the case of NGC 5548, we also checked that a better modelization of the WA (with the CLOUDY code used by Nicastro et al. 2000) does not affect the results on the continuum. We note also that, in the case of NGC 4151, we found smaller errors for the spectral index Γ ($\Delta\Gamma \simeq \pm 0.01$) in comparison to Piro et al. (2000a, where they found $\Delta\Gamma \simeq \pm 0.1$). This is simply due to the fact that the latters have computed the errors using the MECS and PDS data (above 3.5 keV) whereas we have used the LECS, MECS and PDS ones together (thus adding the soft excess parameters in the fitting procedure).

For the PEXRAV model the parameters of the primary continuum determined by the fits are Γ and E_c . The actual physical parameters of the Comptonizing region (also reported in Table 3) have been obtained from the spectral parameters in the following way. The temperature kT_e is simply estimated as $kT_e \equiv E_c/2$, keeping in mind that such approximation roughly holds for $\tau \lesssim 1$. For $\tau \gg 1$, $kT_e \equiv E_c/3$ would be more appropriate. Thus the reported values can be considered as upper limits to the temperature. Knowing the temperature, the optical depth can be computed from the spectral index derived from the PEXRAV fit using the following relation (Shapiro, Lightman & Eardley 1976; Sunyaev & Titarchuk 1980; Lightman & Zdziarski 1987):

$$\Gamma - 1 \simeq \left[\frac{9}{4} + \frac{m_e c^2}{kT_e \tau (1 + \tau/3)} \right]^{1/2} - \frac{3}{2} \quad (1)$$

This equation is valid for $\tau > 1$, and we have checked *a posteriori* that such condition is roughly matched in all cases.

4.2. The slab model

The fits with the AC2 yield directly and consistently the temperature kT_e and optical depth τ , which was our first motivation for starting this approach. The best fit parameters are reported in Table 4. It is worth noting that another parameter enters the fitting procedure in an

important way, that is the temperature of the soft photons, kT_{bb} . Its values (see Table 4) range, in most cases, between 10 and 40 eV and are relatively well constrained with errors of the order of 5-50% whereas we have only data above 100 eV. For large values of kT_{bb} (i.e. $kT_{bb} > 30$ eV), the high energy tail of the black body shape may be detected in the *low energy part* of the BeppoSAX data and kT_{bb} can then be roughly constrained. We recall that the intensity of the seed photon component with respect to the comptonized one is also fixed by the fitted parameters (mainly τ). When no tail is observed, the soft-X-ray data impose, at least, an upper limit of kT_{bb} . For anisotropic geometries, the *high energy part* of the Comptonization spectrum also depends on kT_{bb} , through the location of the anisotropy break. The fitting procedure has thus to adjust kT_{bb} , together with τ , kT_e and R , to reproduce the soft and hard X-ray data resulting in a complex interdependence in the fitting procedure, between the soft and hard part of the spectra.

It is worth noting that, in the case of NGC 4151 96L and 96H, the best fit values of kT_{bb} are relatively large (in fact we have only lower limit, the AC2 working only for $kT_{bb} < 100$ eV). It is true however that in the case of the high state 96H, we don't have any LECS data. Consequently, as explained above, kT_{bb} is not constrained by the soft part of the spectra and large values may be reached. But it is surprising that in the low state 96L, we still find large kT_{bb} , at least 3 times larger than in 1999. A possible explanation is that, in the observation of 1996, the presence of a larger reflection component (also found with the PEXRAV fits) may hide the anisotropy break, thus diminishing the constraints on kT_{bb} , and allowing larger values.

4.3. Comparison between the slab model and PEXRAV

A purely statistical comparison between the two models is not possible since both give acceptable values of χ^2 . The slab model has one more parameter and gives generally lower values of χ^2 , except for NGC 4151. However, we have checked, for this source, that the best fit χ^2 probabilities are similar for the two models. Besides, the two best fits have residuals without significant features and differences between each other. The two models give thus an equivalent representation of the data.

4.3.1. The temperature and optical depth of the corona

For all objects, the estimated corona temperatures (respectively optical depths) from PEXRAV are substantially smaller (respectively larger) than those inferred with an anisotropic Comptonization model. This trend is similar to the result obtained for NGC 5548 by P00. In Fig. 1a we have plotted the corona temperatures obtained with AC2 versus the temperatures obtained with PEXRAV. Large differences (up to a factor 8) are found between the two estimates. Note however that for IC 4329A, for which the high energy data are comparatively better than for the rest of the sample, the two models give results which are quite close to each other.

The reason of these differences is relatively simple. Within PEXRAV type models, the slope of the power law, determined with small errors by the LECS and MECS

data, cannot change, by hypothesis, at higher energies. A cut-off around 100 keV is then required to fit the PDS data. In Comptonization models, the LECS and MECS data determine the slope below the anisotropy break. Above this break the intrinsic spectrum is steeper and thus can fit the PDS data without an additional steepening beyond 100 keV, allowing for a larger temperature and (consequently) a smaller optical depth to keep, roughly, the same power law slope.

4.3.2. The reflection component

The reflection normalizations obtained with AC2 cluster around 1, except for two extreme states of NGC 4151. They are, in all cases but one (ES0 141-G55), larger than those found using the simple cut-off power-law model. We have reported in Fig. 1b the amplitude of the reflection component derived from both models. In some cases we obtain differences of factors 4-5. Note that with the exception of NGC 4151 for all other sources the slab model yields values of R consistent with 1.

The case of NGC 4151 is peculiar, showing a large variation in R between the 96 and 99 observations and an indication of a variation of R also between the low and high states of the July 96 observation. These changes are present irrespective of the model used in the spectral fitting (see also Piro et al. 2000a, 2000b). However the slab model yields higher absolute values, allowing for some reflection also in the 99 observation for which PEXRAV yields $R = 0.01 \pm 0.1$. According to the slab model, the corona temperature is very high in the 99 observation, which may offer a physical connection with the low value of R as discussed in section 5.1.

We can also remark that the relatively small reflection component and the hardness of the spectrum of this object may be difficult to reconcile with simple corona geometries (like a plane or a patchy corona for example). More complex ones (as dynamics coronae for example, Malzac et al. 2000) may be needed. Another possibility may be that the reflecting material in NGC 4151 is highly ionized. In this case, fitting with models which do not take into account the complex ionization pattern of the reflector can severely underestimate the reflection normalization (Balantyne, Ross & Fabian 2000; Done & Nayakshin 2001; .

As an illustration of these results, we have plotted in Fig. 2a and 2b the unfolded best fit spectra of IC4329A and NGC 4151 (observation of 1999) obtained with PEXRAV (dashed lines) and AC2 (solid lines). We have also plotted in each case the reflection hump component to better estimate its contribution to the total spectrum. In the case of IC 4329A, the two models give roughly the same result at high energy. For NGC 4151 however, large differences are expected between PEXRAV and AC2, with a factor of 2-3 at 300 keV and larger than 10 above 500 keV.

5. DISCUSSION

A Comptonizing corona above a passive optically thick layer (approximating an accretion disk with negligible internal heating) is a complex system, in which the soft seed photons for the Comptonization process are produced by reprocessing of the Comptonized emission in

the underlying passive layer. Such a corona is "self-cooled" and, for a given geometrical configuration of the system, can only be in equilibrium if the temperature and optical depth satisfy a definite relation (Haardt & Maraschi 1991). These relations which essentially correspond to roughly constant Compton parameters $y \simeq 4 \left(\frac{kT_e}{m_e c^2} \right) \left[1 + 4 \left(\frac{kT_e}{m_e c^2} \right) \right] \tau(1 + \tau)$, with $y \simeq 0.5$ and 2 for the slab and hemisphere respectively, have been accurately computed by Stern et al. (1995; see also for a review Svensson 1996).

In Fig. 3a and 3b the values of τ vs. kT_e , obtained for the 6 sources considered here using the spectral models AC2 and PEXRAV, are compared with the theoretical relations expected for a Comptonizing region in energy balance for a plane (filled rectangles, solid line) and hemispherical (filled hemispheres, dashed line) configuration respectively.

The best fit results obtained with AC2 (Fig. 3a) are relatively close to the theoretical expectations for the slab case even if they tend to fall preferentially above the solid line. The data therefore indicate a Comptonization parameter larger than for a pure slab geometry, that is a more "photon-starved" configuration. A similar result was already derived by P00 for NGC 5548. For the latter source, best fits with a hemispherical Comptonisation model were also performed. The derived coronal parameters were in fact in good agreement with the theoretical predictions for the hemisphere. However an implausibly large value of the reflection component (of the order of 2) was required, suggesting that the real configuration is more complex than these two ideal cases. For the present sample we did not perform fits with hemispherical models.

The values of kT_e and τ obtained with PEXRAV (cf. Fig. 3b) show the same trend as found with AC2 that is larger values of τ for smaller values of kT_e . They also fall above the theoretical expectation for a slab and even above the theoretical expectation for a hemisphere (the theoretical curves of Stern et al. 1995 have been extended to large τ assuming a constant value of the Compton parameter for each curve i.e. $y \simeq 0.5$ and 2 for the slab and hemispherical configuration respectively). Therefore this set of parameters suggests, for each source of our sample, a configuration more "photon-starved" than a hemisphere.

An important difference with respect to the slab model is that the optical depths derived from PEXRAV fits are generally larger than 1. The corona should then be optically thick reducing or cancelling the effects of anisotropy. Therefore also the PEXRAV model has an internal consistency. However a corona with large optical depth may wash out discrete features from the underlying disk (e.g. lines and reflection itself, Petrucci et al. 2001) more than would be desirable. This problem could be alleviated if the corona was "patchy" (and possibly dynamic cf. section 4.3.2).

We conclude that both a hot, optically thin corona with significant anisotropic effects and a less hot, optically thick, patchy corona with negligible anisotropy are consistent with the available data.

5.1. Correlations between physical parameters

A correlation between the reflection normalization R and the photon index Γ has been claimed by Z99 from the study, using PEXRAV to model the primary continuum, of a large number of GINGA observations of Seyfert and galactic black hole objects. Yet, the validity of this correlation is under debate since R and Γ are strongly correlated in the fitting procedure (Vaughan & Edelson 2000). It seems however more significant and less dispute in the case of the galactic black hole objects where the errors on both parameters are smaller.

We have plotted in Fig. 4 the reflection normalization R versus the photon index Γ we obtained with PEXRAV. In our case, we do not find a clear correlation between the two parameters. A Spearman rank-order correlation test gives inconclusive results with $r_s \simeq 0.3$. However our sample is biased in favor of objects with hard spectra, to ensure a good detection in the PDS instrument. When the 13 objects actually observed by BeppoSAX are taken into account a stronger correlation is observed (M00), in agreement with Z99.

In the case of the AC2 model we have no simple way of characterizing the spectral shape. Also results are available for only 6 sources and we cannot include the other Seyfert 1s observed by BeppoSAX. Therefore a direct comparison with the Z99 correlation is not possible. Below, however, we examine the correlation of R with the corona temperature which can be computed for the two models.

5.1.1. Relation between R or Γ and the temperature of the corona

Z99 interpret the correlation between R and Γ in the framework of thermal reprocessing models where R is directly proportional to the solid angle subtended by the cold matter surrounding the corona. The latter solid angle is not necessarily proportional to the soft photon flux reentering the corona, but it is likely that the larger is R , the larger is the ratio of soft luminosity to hard luminosity in the corona, i.e. the smaller is the Comptonization parameter y , resulting in softer spectra (larger Γ).

It is interesting that the BeppoSAX data can provide the temperatures associated with sources with different values of R or Γ , which were not available from the GINGA data used by Z99. The result is shown in Fig. 5 where we plot R vs. the corona temperature $E_c/2$ obtained with PEXRAV. Here again, in order to have a larger sample, we added the best fit values obtained by M00 for the other Seyfert 1s observed with BeppoSAX. This plot suggests a *positive* correlation between the two parameters, that is, the temperature of the corona is *larger* for *larger* values of the reflection normalization. In fact a plot of $E_c/2$ vs. Γ shows that steeper spectra correspond to higher temperatures and (as a corollary) to lower optical depths (cf. Fig. 6a and 6b).

The slab model analysis yields different trends. A plot of R vs. kT_e for the latter model shows that sources with *larger* R tend to have *lower* kT_e (cf. Fig. 7), a behaviour opposite to what is found with PEXRAV. The

suggested correlation depends however strongly on the different states of NGC 4151.

To summarize, an analysis in terms of PEXRAV indicates the following correlations: *larger* reflection component (steeper Γ) – *larger* temperature (cf. Fig. 5) while the analysis in terms of anisotropic Comptonization yields: *larger* reflection – *lower* temperature (cf. Fig. 7).

The latter behaviour is naturally expected in pair free Compton cooled coronae (see Fig 3a) since the transition to lower Compton parameter (i.e. higher l_s/l_h as suggested by a larger R) implies a decrease in the temperature for constant optical depth, as (relatively well) verified by our sources.

The behaviour indicated by PEXRAV could instead be understood better in the case of a pair dominated corona in pair equilibrium. In such a case, for constant hard compactness, the larger the ratio l_s/l_h , the larger the temperature of the corona. This behavior is simply imposed by the pair equilibrium. Indeed, an increase of the cooling corresponds to a decrease of the number of particles in the hard tail of the thermal particle distribution. To reach a new equilibrium the temperature must increase. (Zdziarski 1985; Svensson 1982; Ghisellini & Haardt 1994 ; Coppi 1999).

A possible limitation of the “pair dominated” interpretation comes from the high values of the compactness l_h required by the physical parameters determined with PEXRAV. We have reported on Fig. 8 the τ – T_e relations expected, for a pair dominated corona, for different values of l_h , but varying the ratio l_h/l_s . We have also included the observations of M00. The data require values of l_h in the range 100–1000. Given the (unabsorbed) luminosity of the sources of our sample ($L_{0.1-200\text{ keV}}$ of the order of $10^{44}\text{ erg.cm}^{-2}\text{.s}^{-1}$), this implies black hole mass upper limits of the order of 10^7 solar masses (for $l_h=100$). This is relatively smaller than (but roughly consistent with) black hole mass estimations obtained from reverberation mapping or resolved kinematics methods for most of the objects of our sample (see Gebhardt et al. 2000 and Nelson 2000 and references therein). The worse case is that of NGC 4151, where the PEXRAV best fit values of kT_e and τ require very large hard compactness (larger than 1000), implying a black hole mass of $\sim 10^5 M_\odot$ (reverberation mapping methods estimate a black hole mass of $\sim 10^7 M_\odot$, Clavel et al. 1987; Ulrich & Horne 1996). In this case, however, the complexity of the soft part of the spectrum may lead to an incorrect modelisation of the continuum. We therefore conclude that the pair dominated coronae interpretation is also still valid for this object. Other observations (with better constraints on the compactness and the physical parameter of the corona) are clearly needed to confirm or disprove these results.

6. CONCLUSION

The aim of this paper was to test anisotropic Comptonization models over the high signal to noise *BeppoSAX* observations of a sample of six Seyfert 1 (seven observations). We use two types of model: a detailed Comp-

tonization code in slab geometry, which treats carefully the anisotropy effects in Compton processes, and a simple cut-off power law plus reflection model (PEXRAV model of XSPEC). The latter is generally used as a zero order approximation to Comptonization spectra. If this is a relatively good approximation for isotropic geometry, it fails to reproduce the real shape of Comptonization spectra in anisotropic ones (like a plane, hemispherical or spherical hot region above a flat disk). In this case, due to the deficiency of the first order scattering component towards the observer, it better resembles a broken power law with convex curvature. This leads to strong differences between the best fit parameter values obtained with these two models. The main results of this work are the following:

- The data are well fitted by both models and there is no statistical evidence for a model to be better than the other. Both models give results in agreement with a X-ray source geometry more “photon starved” than the slab case.
- Our best fits with Comptonization models in slab geometry give a temperature generally much larger and an optical depth much smaller than derived from the power law + cut-off fits, using standard Comptonization formulae. The estimate of the reflection normalization is also larger with the slab corona model.
- The two models also lead to different relationships between physical parameters. For instance, PEXRAV indicates a correlation between the reflection normalization and the corona temperature whereas the slab corona model suggests an anticorrelation. This has major consequences for the physical interpretation of the data. Thus, the PEXRAV results suggest that the hot corona may be pair dominated whereas the slab corona model is in better agreement with a low pair density solution.

These results should have observational consequences. First, the large differences in the fitted temperatures lead to widely different predictions as to the fluxes emitted at higher energies, above the PDS range. This underlines the need of better soft γ -ray observations, as those possibly provided by INTEGRAL, in order to directly confirm or disprove the temperatures inferred with anisotropic Comptonization models.

On the other hand, the large values of τ predicted by PEXRAV would spread out the reflection hump in the entire X-ray range, avoiding any detection of this component. The fact that we obtain not negligible values of R with PEXRAV may however be reconciled with the large values of τ if the corona is “patchy”. Indeed, in this case, reflection could come from the uncovered part of the cold, reflecting material. Part of the reflection could also come from the torus. The variability of the reflection component may allow to differentiate these two possibilities. Large values of τ would also modify the profile of the Fe line component produced in the disk, leading to an attenuation and broadening of the line. Forthcoming observations with CHANDRA and XMM-Newton are expected to bring substantial progress on this issue.

Acknowledgements: POP acknowledges a grant of the European Commission under contract number ERBFMRX-CT98-0195 (TMR network "Accretion onto black holes, compact stars and protostars"). This work was par-

tially supported by the Italian MURST through the grant COFIN98-02-15-41 (JM) and by the Agenzia Spaziale Italiana (ASI) through the grant ASI-ARS-99-74 (LM,FH).

REFERENCES

- Arnaud, K. A. 1996, ASP Conf. Ser. 101: Astronomical Data Analysis Software and Systems V, 5, 17
- Ballantyne, D. R., Ross, R. R., & Fabian, A. C. 2000, MNRAS in press (astro-ph/0102040)
- Boella, G., et al. 1997, A&AS, 122, 327
- Cappi, M., Mihara, T., Matsuoka, M., Hayashida, K., Weaver, K. A. and Otani, C. 1996, ApJ, 458, 149
- Clavel, J. et al. 1987, ApJ, 321, 251
- Coppi, P. 1999, proceedings of the workshop "High Energy Processes in Accreting Black Holes", eds. J. Poutanen and R. Svensson, ASP Conf. Series, Vol. 161, p. 375
- De Rosa et al., 2000, in preparation.
- Done, C., Pounds, K. A., Nandra, K. and Fabian, A. C. 1995, MNRAS, 275, 417
- Done, C. & Nayakshin, S. 2001, ApJ, 546, 419
- Elvis, M., Briel, U. G. & Henry, J. P. 1983, ApJ, 268, 105
- Elvis, M., Wilkes, B. J. and Lockman, F. J. 1989, AJ, 97, 777
- Evans, I. N., Tsvetanov, Z., Kriss, G. A., Ford, H. C., Caganoff, S. and Koratkar, A. P. 1993, ApJ, 417, 82
- Fiore, F., Guainazzi, M., & Grandi, P. 1999, SAXabc, version 1.2, Cookbook for BeppoSAX NFI Spectral Analysis (BeppoSAX Sci. Data Cont.)
- Frontera, F., Costa, E., Dal Fiume, D., Feroci, M., Nicastro, L., Orlandini, M., Palazzi, E. & Zavattini, G. 1997, A&AS, 122, 357
- Gebhardt, K. et al. 2000, ApJ, 543, L5
- George, I. M., Turner, T. J. & Netzer, H. 1995, ApJ, 438, L67
- George, I. M., Turner, T. J., Mushotzky, R., Nandra, K. and Netzer, H. 1998, ApJ, 503, 174
- George, I. M., Turner, T. J., Netzer, H., Nandra, K., Mushotzky, R. F. and Yaqoob, T. 1998, ApJS, 114, 73
- Ghisellini, G. & Haardt, F. 1994, ApJ, 429, L53
- Ghisellini, G., Haardt, F. & Matt, G. 1994, MNRAS, 267, 743
- Gondek, D., Zdziarski, A. A., Johnson, W. N., George, I. M., McNaron-Brown, K., Magdziarz, P., Smith, D. and Gruber, D. E. 1996, MNRAS, 282, 646
- Haardt, F. & Maraschi, L. 1991, ApJ, 380, L51
- Haardt, F. 1993, ApJ, 413, 680
- Haardt, F. 1994, PhD dissertation, SISSA, Trieste
- Haardt, F., Maraschi, L. & Ghisellini, G. 1997, ApJ, 476, 620
- Holt, S. S., Mushotzky, R. F., Boldt, E. A., Serlemitsos, P. J., Becker, R. H., Szymkowiak, A. E. and White, N. E. 1980, ApJ, 241, L13
- Jourdain, E. et al. 1992, A&A, 256, L38
- Kaspi, S., Brandt, W. N., Netzer, H., Sambruna, R., Chartas, G., Garmire, G. P. and Nousek, J. A. 2000, ApJ, 535, L17
- Lightman, A. P. & Zdziarski, A. A. 1987, ApJ, 319, 643
- Lightman, A. P. & White, T. R. 1988, ApJ, 335, 57
- Madejski, G. M. et al. 1995, ApJ, 438, 672
- Maisack, M. et al. 1993, ApJ, 407, L61
- Magdziarz, P. & Zdziarski, A. A. 1995, MNRAS, 273, 837
- Malzac J., Beloborodov, A. & Poutanen, J. A&A, submitted
- Matt, G., to appear in the proceedings of "X-Ray Astronomy '99", 1999, September 6-10, Bologna (Italy), (M00, astro-ph/0007105)
- Matsuoka, M., Piro, L., Yamauchi, M. & Murakami, T. 1990, ApJ, 361, 440
- Morse, J. A., Wilson, A. S., Elvis, M. & Weaver, K. A. 1995, ApJ, 439, 121
- Nandra, K. & Pounds, K. A. 1994, MNRAS, 268, 405
- Nandra, K., George, I. M., Mushotzky, R. F., Turner, T. J. and Yaqoob, T. 1997, ApJ, 477, 602
- Nelson, C. H. 2000, ApJ, 544, L91
- Nicastro, F. et al. 2000, ApJ, 536, 718
- Ogle, P. M., Marshall, H. L., Lee, J. C. & Canizares, C. R. 2000, ApJ, in press (astro-ph/0010314)
- Parmar, A. N., et al. 1997, A&AS, 122, 309
- Perola, G. C. et al. 1999, A&A, 351, 937
- Perola, G. C. et al. 1986, ApJ, 306, 508
- Perola, G. C. et al. 2000, A&A, 358, 117 (PER00)
- Petre, R., Mushotzky, R. F., Holt, S. S. and Krolik, J. H. 1984, ApJ, 280, 499
- Petrucchi, P. O. et al. 2000, ApJ, 540, 131 (P00)
- Petrucchi, P. O., A. Merloni, A. Fabian et al., 2001, in preparation
- Piro, L., Yamauchi, M. & Matsuoka, M. 1990, ApJ, 360, L35
- Piro, L., Matt, G. and Ricci, R. 1997, A&AS, 126, 525
- Piro et al. 1999, Proc. of the 32 COSPAR Ass., Session E1.1 "Broad Band X-Ray Spectra of Cosmic Sources, eds K. Makishima, L. Piro, T. Takahashi, Advances in Space Research (astro-ph/9908360)
- Piro, L. et al. 2000a, A&A, submitted
- Piro, L. et al. 2000b, Advances in Space Research, 25, 453
- Pounds, K. A., Warwick, R. S., Culhane, J. L. and de Korte, P. A. J. 1986, MNRAS, 218, 685
- Pounds, K. A., Nandra, K., Stewart, G. C., George, I. M. and Fabian, A. C. 1990, Nature, 344, 132
- Reynolds, C. S. 1997, MNRAS, 286, 513
- Shapiro, S. L., Lightman, A. P. & Eardley, D. M. 1976, ApJ, 204, 187
- Stern, B. E., Poutanen, J., Svensson, R., Sikora, M. & Begelman, M. C. 1995, ApJ, 449, L13
- Sunjaev, R. A. & Titarchuk, L. G. 1980, A&A, 86, 121
- Svensson, R. 1982, ApJ, 258, 335
- Svensson, R. 1996, A&AS, 120, C475
- Turner, T. J. & Pounds, K. A. 1989, MNRAS, 240, 833
- Turner, T. J., George, I. M. and Mushotzky, R. F. 1993, ApJ, 412, 72
- Turner, T. J., Nandra, K., George, I. M., Fabian, A. C. & Pounds, K. A. 1993, ApJ, 419, 127
- Ulrich, M. & Horne, K. 1996, MNRAS, 283, 748
- Vaughan, S. & Edelson, R., ApJ, in press (astro-ph/0010274)
- Walter, R. & Fink, H. H. 1993, A&A, 274, 105
- White, T. R., Lightman, A. P. & Zdziarski, A. A. 1988, ApJ, 331, 939
- Zdziarski, A. A. & Lightman, A. P. 1985, ApJ, 294, L79
- Zdziarski, A. A., Johnson, W. N., Done, C., Smith, D. and McNaron-Brown, K. 1995, ApJ, 438, L63
- Zdziarski, A. A., Lubinski, P. and Smith, D. A. 1999, MNRAS, 303, L11 (Z99)

Source Name	Observation Date	Exposure Time (ks)	PDS Detection	References
NGC 5548	Aug. 97	300	55	Nicastro et al. 2000
IC4329A	Jan. 98	100	68	Perola et al. 1999
NGC 4151	Jan. 99	100	182	Piro et al. 2000a
	Jul. 96L	56	130	Piro et al. 2000a, 2000b
	Jul. 96H	15	90	Piro et al. 2000a, 2000b
ESO 141-G55	Nov. 99	100	15	-
Mkn 509	May/Oct 98	100	29	Perola et al. 2000
NGC 3783	Jun. 98	300	55	De Rosa et al. 2000

TABLE 1

SOURCES NAMES, OBSERVATIONS DATES AND EXPOSURES OF OUR SAMPLE. WE HAVE ALSO REPORTED THE STATISTICAL SIGNIFICANCE IN σ OF PDS DETECTION IN 13–300 KEV BAND. WE HAVE ALSO REPORTED, AS FAR AS POSSIBLE, THE REFERENCES PRESENTING THE FIRST DATA ANALYSIS OF EACH OBSERVATION.

$N_H(10^{20}\text{cm}^{-2})^a$	E_{line}^b	σ_{line}	E_1^b	τ_1	E_2^b	τ_2
$0.8^{+0.5}_{-0.6}$	$0.55^{+0.03}_{-0.1}$	$0.1^{+0.05}_{-0.04}$	$0.84^{+0.02}_{-0.02}$	$0.63^{+0.09}_{-0.04}$	$1.31^{+0.10}_{-0.03}$	$0.16^{+0.04}_{-0.04}$

TABLE 2

BEST FIT PARAMETER OF THE SOFT X-RAY COMPLEX OF NGC 3783, I.E. TWO EDGES AND AN EMISSION LINE (SEE TEXT FOR DETAILS), OBTAINED WITH PEXRAV. WE HAVE ALSO REPORTED THE BEST FIT COLUMN DENSITY, IN EXCESS OF THE GALACTIC ONE.

^ain excess of $N_{H,Gal.} = 8.5 \times 10^{20} \text{ cm}^{-2}$

^bin keV

Source	Γ	$kT_e = \frac{E_c}{2}$	τ	R	N_h	χ^2
NGC 5548	$1.59^{+0.01}_{-0.02}$	65^{+20}_{-15}	$2.2^{+0.5}_{-0.4}$	$0.5^{+0.2}_{-0.1}$	$0.015^{+0.002}_{-0.001}$	147/171
IC 4329 A	$1.81^{+0.01}_{-0.02}$	105^{+40}_{-20}	$1.1^{+0.2}_{-0.3}$	$0.3^{+0.1}_{-0.1}$	$0.40^{+0.02}_{-0.02}$	161/171
NGC 4151 99	$1.45^{+0.15}_{-0.05}$	45^{+25}_{-5}	$3.4^{+0.6}_{-1.4}$	$0.01^{+0.1}_{-0}$	$N_{H1} = 7.0^{+0.5}_{-1.5} N_{Hcov} = 18^{+2}_{-3}$ $f_{cov} = 0.60^{+0.05}_{-0.05}$	177/179
NGC 4151 96L	$1.24^{+0.01}_{-0.01}$	30^{+3}_{-3}	$7.0^{+0.3}_{-0.8}$	$0.45^{+0.12}_{-0.05}$	$N_{H1} = 3.5^{+0.9}_{-0.2} N_{Hcov} = 17^{+3}_{-1}$ $f_{cov} = 0.65^{+0.05}_{-0.05}$	106/83
NGC 4151 96H	$1.28^{+0.01}_{-0.11}$	30^{+5}_{-2}	$6.1^{+2.9}_{-0.7}$	$0.2^{+0.1}_{-0.1}$	$N_{H1} = 5^{+1}_{-1}$	61/53
ESO 141-G55	$1.9^{+0.04}_{-0.05}$	65^{+180}_{-25}	$1.4^{+0.8}_{-0.9}$	$1.7^{+0.8}_{-0.6}$	$0.058^{+0.006}_{-0.005}$	176/162
Mkn 509	$1.60^{+0.03}_{-0.03}$	40^{+15}_{-10}	$3.1^{+0.8}_{-0.8}$	$0.7^{+0.3}_{-0.3}$	$0.048^{+0.001}_{-0.002}$	163/202
NGC 3783	$1.62^{+0.01}_{-0.02}$	55^{+15}_{-10}	$2.3^{+0.4}_{-0.4}$	$0.3^{+0.2}_{-0.1}$	$0.093^{+0.005}_{-0.006}$	151/162

TABLE 3

BEST FIT PARAMETERS USING THE PEXRAV MODEL: THE PHOTON INDEX Γ , THE TEMPERATURE kT_e (IN KEV) AND OPTICAL DEPTH τ OF THE CORONA, THE REFLECTION NORMALIZATION R AND THE BEST FIT TOTAL (I.E. INTRINSIC+GALACTIC, IN 10^{22} cm^{-2}) COLUMN DENSITY FOR EACH OBJECT. IN THE CASE OF NGC 4151, THE COMPLEX NEUTRAL ABSORBER IS DETAILED IN SECTION 3.2.1. THE COMPUTATION OF kT_e AND τ ARE EXPLAINED IN SECTION 4.1.

Source	kT_e	τ	kT_{bb}	R	N_h	χ^2
NGC 5548	230^{+10}_{-5}	$0.18^{+0.01}_{-0.01}$	22^{+3}_{-2}	$0.9^{+0.1}_{-0.1}$	$0.027^{+0.011}_{-0.009}$	144/170
IC4329A	170^{+10}_{-5}	$0.20^{+0.01}_{-0.01}$	15^{+3}_{-2}	$1.0^{+0.3}_{-0.1}$	$0.35^{+0.01}_{-0.02}$	158/170
NGC 4151 99	315^{+10}_{-5}	$0.08^{+0.15}_{-0.01}$	20^{+8}_{-1}	$0.25^{+0.10}_{-0.05}$	$N_{H1} = 7.5^{+0.5}_{-0.5} N_{Hcov} = 19^{+1}_{-1}$ $f_{cov} = 0.6^{+0.2}_{-0.1}$	184/178
NGC 4151 96L	170^{+80}_{-10}	$0.20^{+0.05}_{-0.10}$	>60	$1.8^{+0.9}_{-0.4}$	$N_{H1} = 4.3^{+0.3}_{-0.6} N_{Hcov} = 20^{+2}_{-5}$ $f_{cov} = 0.65^{+0.05}_{-0.05}$	115/82
NGC 4151 96H	190^{+40}_{-10}	$0.18^{+0.11}_{-0.01}$	>90	$1.1^{+0.5}_{-0.1}$	$N_{H1} = 7.0^{+0.5}_{-1}$	66/52
ESO 141-G55	260^{+30}_{-30}	$0.05^{+0.01}_{-0.01}$	25^{+3}_{-3}	$1.1^{+0.1}_{-0.3}$	$0.09^{+0.02}_{-0.02}$	166/161
Mkn 509	210^{+20}_{-30}	$0.17^{+0.06}_{-0.03}$	38^{+7}_{-8}	$1.0^{+0.6}_{-0.4}$	$0.07^{+0.01}_{-0.01}$	164/201
NGC 3783	265^{+15}_{-5}	$0.12^{+0.03}_{-0.01}$	13^{+2}_{-3}	$0.7^{+0.2}_{-0.3}$	$0.11^{+0.07}_{-0.02}$	143/161

TABLE 4

BEST FIT PARAMETERS USING THE COMPTONIZATION MODEL OF H94: THE TEMPERATURE AND OPTICAL DEPTH OF THE CORONA kT_e (IN KEV) AND τ , THE SOFT PHOTON TEMPERATURE kT_{bb} (IN eV), THE REFLEXION NORMALIZATION R AND THE BEST FIT TOTAL (I.E. INTRINSIC+GALACTIC, IN 10^{22} cm^{-2}) COLUMN DENSITY FOR EACH OBJECT. IN THE CASE OF NGC 4151, THE COMPLEX NEUTRAL ABSORBER IS DETAILED IN SECTION 3.2.1.

Figure Captions

FIG. 1.— (a) Best fit values of the corona temperatures obtained with the cut-off power law + reflection model PEXRAV versus the best fit values obtained with the Comptonization model in slab geometry H94. (b) Same as (a) but with the best fit values of the reflection normalization. The filled squares represent the different observations of NGC 4151.

FIG. 2.— (a) Unfolded best fit spectra of IC 4329A with PEXRAV (dashed lines) and H94 (solid lines). For each model, we have also plotted the continuum without the reflection contribution and the reflection hump. (b) Same as (a) but for the observation of 1999 of NGC 4151.

FIG. 3.— Optical depth τ versus temperature kT_e from (a) H94 and (b) PEXRAV fits. The theoretical relations between τ and kT_e for a plane and hemispherical Comptonizing region in energy balance, for $kT_{bb}=5$ eV, are shown for comparison in solid and dashed line respectively (filled rectangles and hemispheres are from Stern et al. 1995. These theoretical relations have been extended to large optical depth assuming the constancy of the Compton parameter, cf. section 5). The filled squares represent the different observations of NGC 4151.

FIG. 4.— Reflection R versus photon index Γ from PEXRAV. The open symbols are from M00 while the solid ones are the results of this work. The filled squares represent the different observations of NGC 4151.

FIG. 5.— Reflection component R versus corona temperature $E_c/2$ from PEXRAV. The open symbols are from M00 while the solid ones are the results of this work. The filled squares represent the different observations of NGC 4151.

FIG. 6.— (a) PEXRAV corona temperature $E_c/2$ and (b) PEXRAV corona optical depth τ versus photon index Γ . The open symbols are from M00 while the solid ones are the results of this work. The filled squares represent the different observations of NGC 4151.

FIG. 7.— Reflection normalization R versus corona temperature kT_e obtained with the slab model. The filled squares represent the different observations of NGC 4151.

FIG. 8.— Same as Fig. 3 but with extra τ - kT_e curves expected in the case of a pair dominated spherical corona for constant values of the hard compactness (in dot-dashed lines. From left to right, $l_h=1000$, 100 and 10) but varying the starvness ratio l_s/l_h . We have added the data from M00 in open symbols while the solid ones are the results of this work. The filled squares represent the different observations of NGC 4151.

Figures

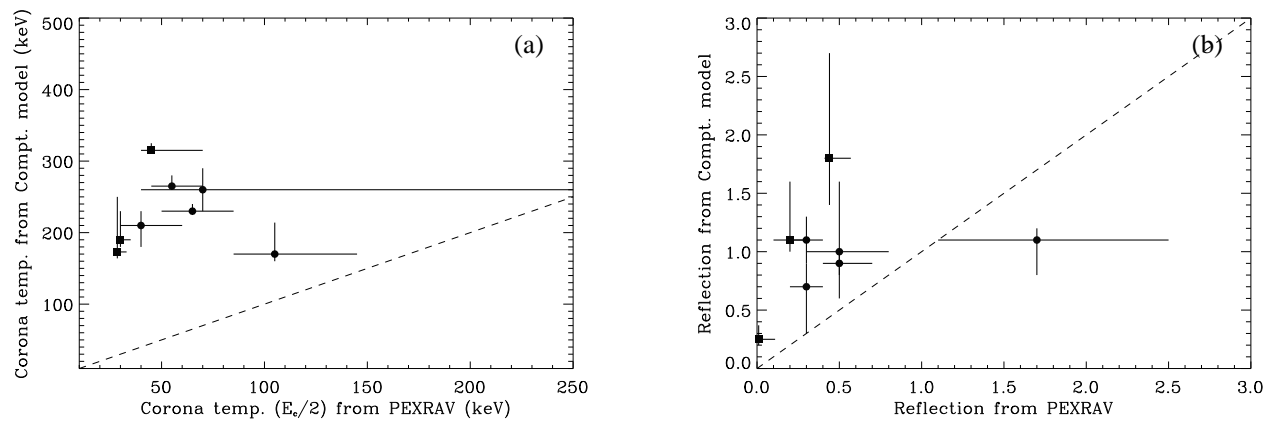


FIG. 1.—

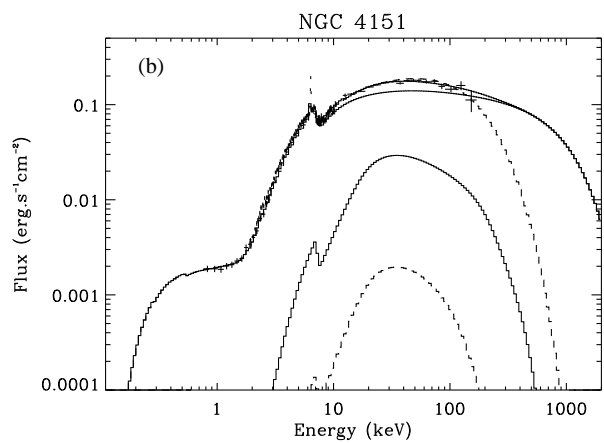
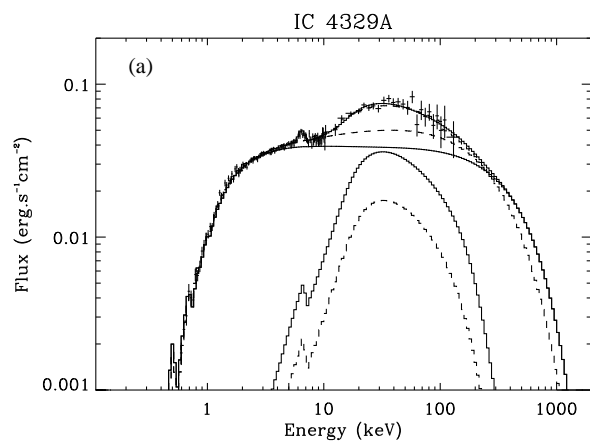


FIG. 2.—

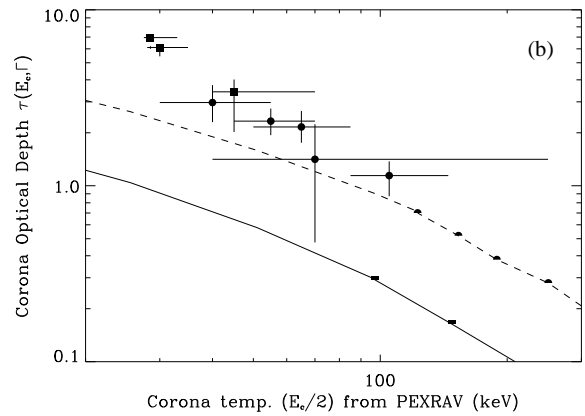
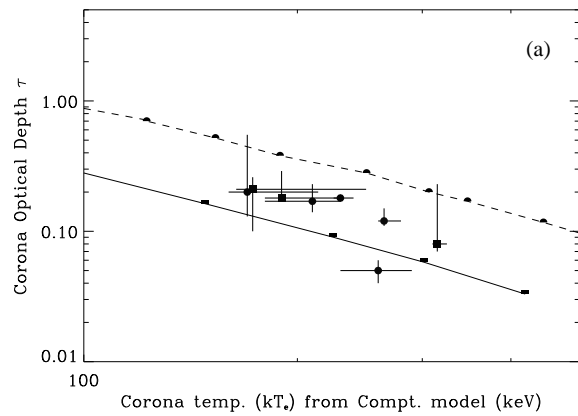


FIG. 3.—

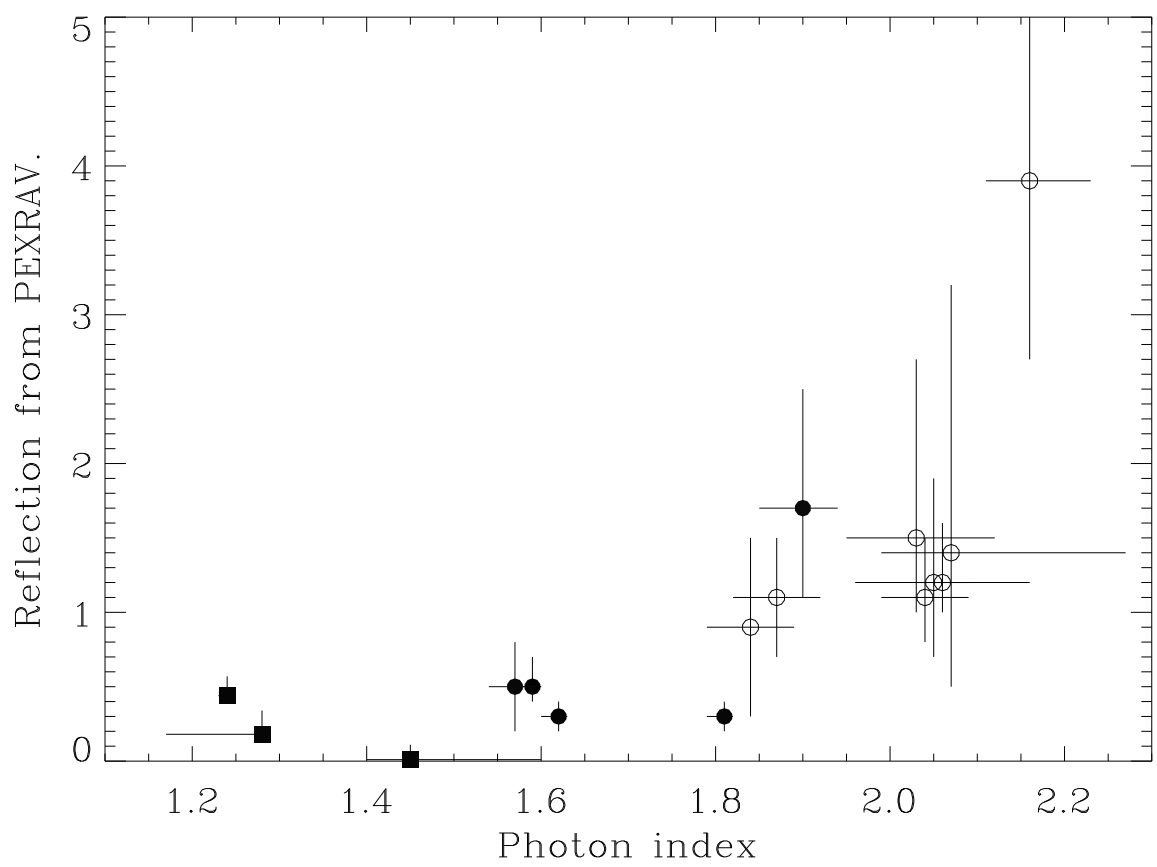


FIG. 4.—

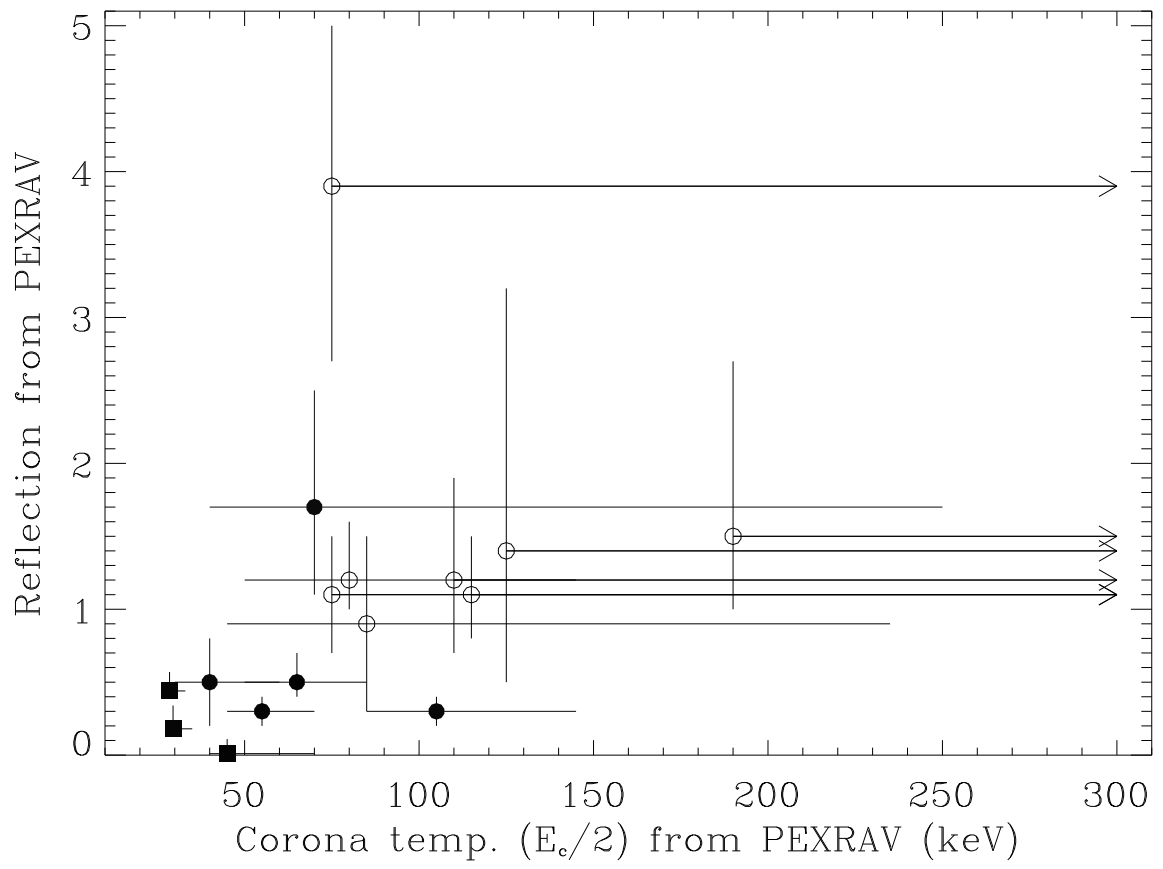


FIG. 5.—

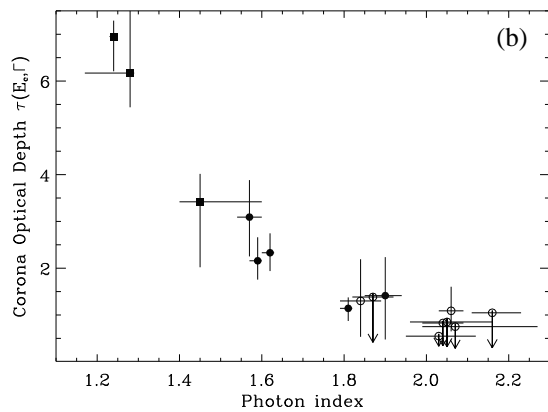
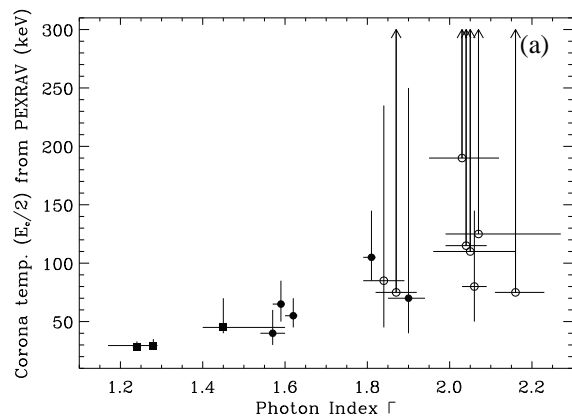


FIG. 6.—

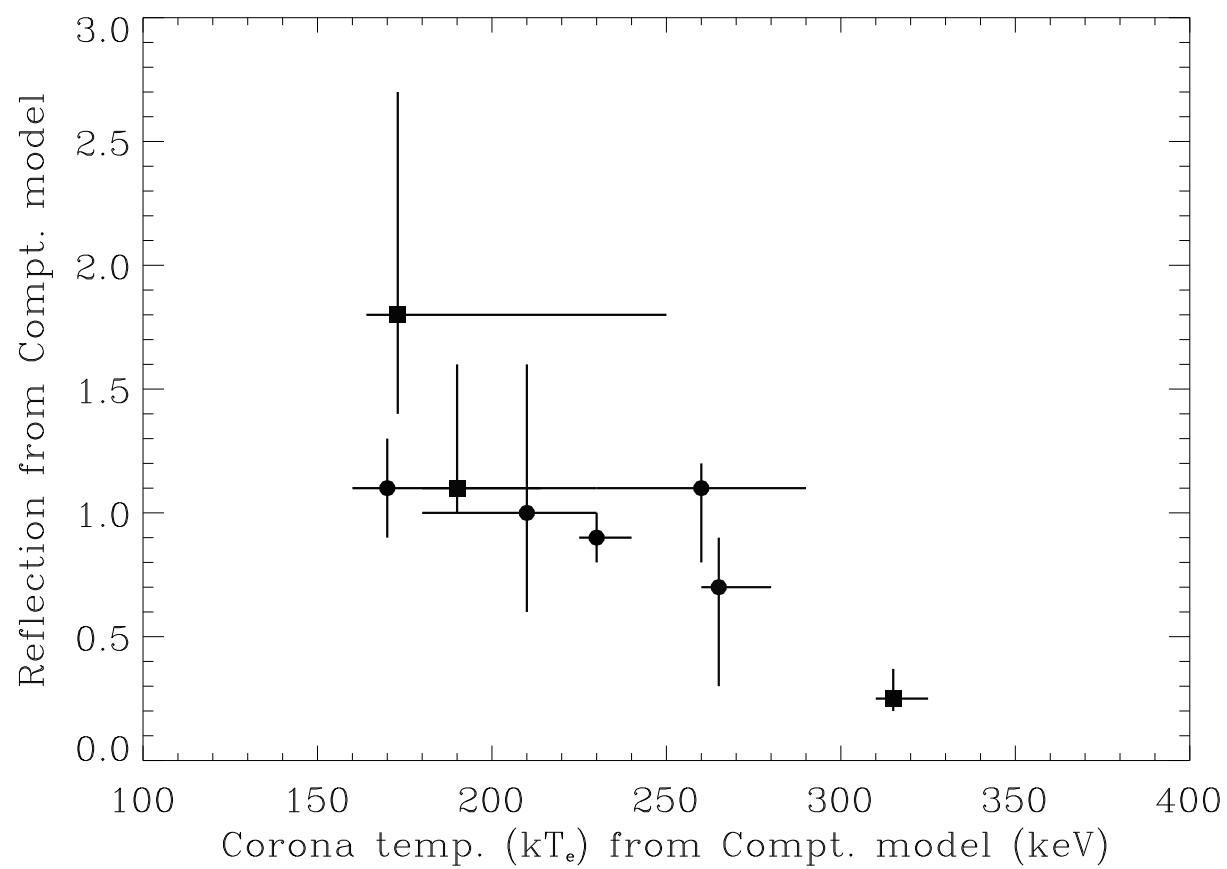


FIG. 7.—

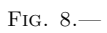


FIG. 8.—